J Mater Sci

Metals & corrosion

Dislocation–grain boundary interactions in Ta: numerical, molecular dynamics, and machine learning approaches

A. Kedharnath[1,2,*], Rajeev Kapoor[1,2], and Apu Sarkar[1,2]

[1] *Mechanical Metallurgy Division, Bhabha Atomic Research Centre, Mumbai 400085, India*
[2] *Division of Engineering Sciences, Homi Bhabha National Institute, Anushaktinagar, Mumbai 400094, India*

Received: 25 September 2023
Accepted: 11 November 2023

ABSTRACT

The motivation of this work was to find the appropriate molecular dynamics (MD) and slip transmission parameters of dislocation–grain boundary (GB) interaction in tantalum that correlate with the stress required for the grain boundary to deform. GBs were modeled using [$\overline{1}12$], [$\bar{1}10$], and [111] as rotation axes and rotation angle between 0° and 90°. Dislocation on either {110} or {112} slip planes was simulated to interact with various GB configurations. Drop in shear stress, drop in potential energy, critical distance between dislocation and GB, and critical shear stress for dislocation absorption by the GB were the parameters calculated from MD simulations of dislocation–GB interactions. Machine learning models eXtreme Gradient Boosting and SHapley Additive exPlanations (SHAP) were used to find the correlation between the various parameters and yield stress of the GB configurations. Machine learning results showed that the MD parameters—critical distance between the dislocation and GB, drop in shear stress; and slip transmission parameter—m' have a stronger correlation with yield stress. The SHAP results sorted the prominent slip plane and rotation axis affecting the yield stress. The configurations with dislocation on {112} slip plane, and configurations with [111] rotation axis were difficult to deform (higher yield stress of GB) than {110} slip plane and [$\overline{1}12$] and [$\bar{1}10$] rotation axes configurations.

Handling Editor: Ghanshyam Pilania.

Address correspondence to E-mail: kedharnath1992@gmail.com; kedharnath@barc.gov.in

https://doi.org/10.1007/s10853-023-09167-y
Published online: 21 December 2023

GRAPHICAL ABSTRACT

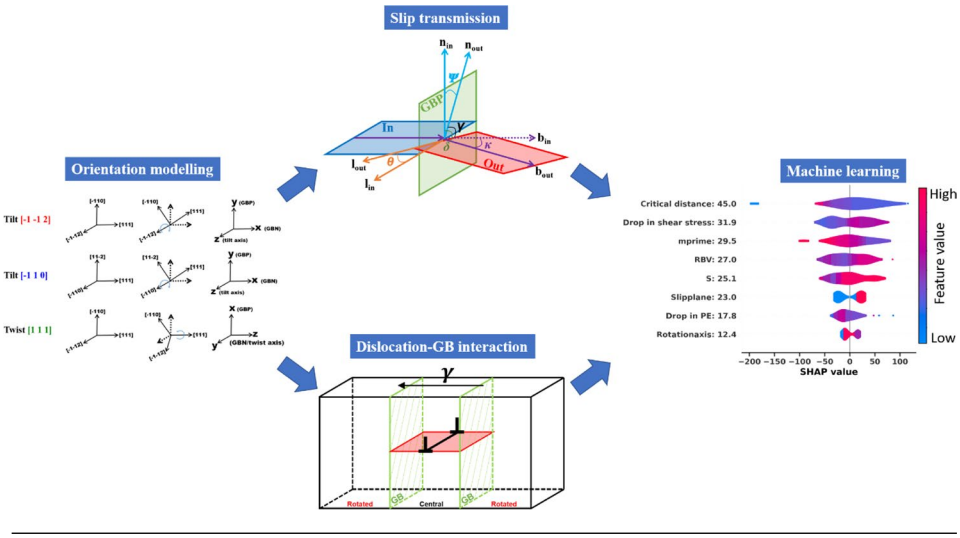

Introduction

The plastic deformation of crystalline materials is governed by the movement of a large number of dislocations. By creating obstacles to dislocations, the strength of a material can be improved. Obstacles can be other dislocations, grain boundaries (GBs), precipitates, or solute atoms. Dislocation–GB interaction plays an important role in the GB strengthening mechanism. The type of interactions dislocations have with GBs determine their strengthening ability. The interactions can be either the pileup mechanism, absorption of dislocation in the GB, or transmission of the dislocation to the neighboring grain. These interactions depend on the dislocation and GB types. Hall–Petch relation [1], which relates the yield strength of the material with the GB spacing, lacks the knowledge of the type of GB. Electron microscopic experiments [2–7] and atomistic simulations [8–13] have been carried out to understand the dislocation–GB interaction, specifically the slip transmission through various GBs. The slip transmission was quantified through slip transmission parameters (STPs) based on the crystallographic orientation of the bicrystals forming the GB. The barrier for dislocations to transmit through Σ GBs was found to be dependent on their GB energies [14]. Kacher et al. concluded that the residual strain in the GB of titanium was the primary parameter for slip transmission irrespective of the type of dislocation [15]. Guo et al. found a cutoff value of 0.7 for the modified m' parameter below which slip transmission was difficult [3]. Patriarca et al. identified strain field and residual burger vector (RBV which is the magnitude of the difference between the Burgers vectors of the incoming and outgoing dislocations) to be the promising parameters to study dislocation—GB interactions in bcc FeCr [2]. These experimental results helped us understand the effect of GB types on slip transmission. However, the researchers also reported ambiguity in the STPs. Hansen et al. did not find a correlation between modified m' and RBV parameters with the GB dislocation density [16]. Bieler et al. found scatter in the observed and theoretical results of slip transfer for bcc Ta [4]. Bayerschen et al. opened several questions on the use of these parameters from experimental and computational points of view for general types of GBs other than Σ GBs [17]. The usefulness of these STPs in identifying the slip transmission with various slip planes of bcc materials is still not studied.

Molecular dynamics (MD) technique is a powerful tool for studying atomistic behavior of materials [18–22]. Spearot et al. brought out the challenges in MD simulations and showed that most of the investigations were in Σ GBs [23]. Tsuru et al. found that the results of atomistic simulations of slip transmission through Σ3 GBs were in contrast to the predictions by STPs [24]. Kapoor et al. performed dislocation dynamics simulations of dislocations

interaction with low angle GBs (LAGBs) and found that the shear stress to overcome the GB followed the Hall–Petch relation [25]. There is a need for studying other types of GBs for their slip-resistance property. Though the above-mentioned experiments and simulations studies provided a reasonable understanding on the dislocation–GB interactions, the relation between STPs and the strength of a material is still unresolved. This is essential for understanding the physical meaning of the STPs.

The motivation of this article is to find the appropriate dislocation–GB interaction parameters that best represent the yield stress of the GB with dislocation on either {110} or {112} slip planes in bcc tantalum. To do this, numerical calculations of STPs, MD simulations of dislocation–GB interactions, and explainable machine learning (ML) approaches were used. STPs available in the literature were numerically calculated. MD, a versatile atomistic simulation technique to study the mechanical behavior of metallic systems at the atomic level [26], was used for simulating the dislocation–GB interactions. The slip transmission parameters and parameters computed from MD simulations were used as input to eXtreme Gradient Boosting (XGBoost) [27] and SHapley Additive exPlanations (SHAP) [28] to determine and explain which of these parameters most importantly affect the yield stress of the GB.

Methodology

The article contains three parts—dislocation–GB interaction using MD simulations, numerical calculations of STPs, and feature analysis using ML. Each sub-section will detail each part of the work. The orientations of the grains and GB configurations were similar in MD simulations and numerical calculations of STPs.

Slip transmission parameters

Slip transmission through GBs can be quantified using parameters based on the vectors shown in Fig. 1a. In the numerical calculations, a non-inclined bicrystal GB configuration was used with one grain (IN) containing the in-coming dislocation and the other neighboring grain (OUT) was rotated about either $[\overline{1}12]/[\overline{1}10]/[111]$ axes as shown in Fig. 1b. The dislocation was modeled to slip on either the {110} or {112} planes as shown in Fig. 1c resulting in 64 data points of various STPs (32 configurations with each configuration having either the {110} or {112} slip plane, thus making 64 such configurations).

As the orientation of the IN grain was fixed, the vectors $\boldsymbol{n}_{\mathbf{in}}$, $\boldsymbol{b}_{\mathbf{in}}$, and $\boldsymbol{l}_{\mathbf{in}}$ were fixed for a slip system. Depending on the rotation of the neighboring grain, the vectors $\boldsymbol{n}_{\mathbf{out}}$, $\boldsymbol{b}_{\mathbf{out}}$, and $\boldsymbol{l}_{\mathbf{out}}$ changed and so the angle between these vectors changed which led to the change in the values of the STP. The STPs are listed here:

$$m' = \left(\boldsymbol{n}_{\mathbf{in}} \cdot \boldsymbol{n}_{\mathbf{out}}\right)\left(\boldsymbol{b}_{\mathbf{in}} \cdot \boldsymbol{b}_{\mathbf{out}}\right) = \cos\psi \cos\kappa \tag{1}$$

$$\begin{aligned} N =& \left(\boldsymbol{n}_{\mathbf{in}} \cdot \boldsymbol{n}_{\mathbf{out}}\right)\left(\boldsymbol{b}_{\mathbf{in}} \cdot \boldsymbol{b}_{\mathbf{out}}\right) + \left(\boldsymbol{n}_{\mathbf{in}} \cdot \boldsymbol{b}_{\mathbf{out}}\right)\left(\boldsymbol{b}_{\mathbf{in}} \cdot \boldsymbol{n}_{\mathbf{out}}\right) \\ =& \cos\psi \cos\kappa + \cos\gamma \cos\delta \end{aligned} \tag{2}$$

$$\mathrm{LRB} = \left(\boldsymbol{l}_{\mathbf{in}} \cdot \boldsymbol{l}_{\mathbf{out}}\right)\left(\boldsymbol{b}_{\mathbf{in}} \cdot \boldsymbol{b}_{\mathbf{out}}\right) = \cos\theta \cos\kappa \tag{3}$$

$$s = \left(\boldsymbol{n}_{\mathbf{in}} \cdot \boldsymbol{n}_{\mathbf{out}}\right)\left(\boldsymbol{b}_{\mathbf{in}} \cdot \boldsymbol{b}_{\mathbf{out}}\right)\left(\boldsymbol{l}_{\mathbf{in}} \cdot \boldsymbol{l}_{\mathbf{out}}\right) = \cos\psi \cos\kappa \cos\theta \tag{4}$$

$$\begin{aligned} \lambda =& \cos\left(\frac{90^{\circ}}{\psi_c}\arccos\left(\boldsymbol{n}_{\mathbf{in}} \cdot \boldsymbol{n}_{\mathbf{out}}\right)\right)\cos\left(\frac{90^{\circ}}{\kappa_c}\arccos\left(\boldsymbol{b}_{\mathbf{in}} \cdot \boldsymbol{b}_{\mathbf{out}}\right)\right) \\ =& \cos\left(\frac{90^{\circ}\psi}{\psi_c}\right)\cos\left(\frac{90^{\circ}\kappa}{\kappa_c}\right), \end{aligned} \tag{5}$$

where ψ_c and κ_c are critical values for slip transmission, taken to be $\psi_c = 15°$ and $\kappa_c = 45°$ [29]. Resolved shear stress (RSS) was calculated using the rotation of the applied stress state $\boldsymbol{\sigma}_{applied}$ onto the rotated OUT grain as,

$$\mathrm{RSS} = \left(\boldsymbol{\sigma}_{\mathrm{rotate}} \cdot \boldsymbol{n}_{\mathbf{out}}\right) \cdot \boldsymbol{b}_{\mathbf{out}} = \left(\left(\boldsymbol{R}\boldsymbol{\sigma}_{\mathrm{applied}}\boldsymbol{R}^{\mathbf{T}}\right) \cdot \boldsymbol{n}_{\mathbf{out}}\right) \cdot \boldsymbol{b}_{\mathbf{out}}, \tag{6}$$

where $\boldsymbol{R}$ is the rotation matrix [30] calculated with rotation angle θ_r and rotation axis $\mathbf{t}$ as [30],

$$\begin{aligned} \boldsymbol{R} =& \cos\theta_r \begin{vmatrix} 1 & 0 & 0 \\ 0 & 1 & 0 \\ 0 & 0 & 1 \end{vmatrix} + \left(1 - \cos\theta_r\right) \begin{vmatrix} t_1^2 & t_1t_2 & t_1t_3 \\ t_2t_1 & t_2^2 & t_2t_3 \\ t_3t_1 & t_3t_2 & t_3^2 \end{vmatrix} \\ &+ \sin\theta_r \begin{vmatrix} 0 & -t_3 & t_2 \\ t_3 & 0 & -t_1 \\ -t_2 & t_1 & 0 \end{vmatrix}, \end{aligned} \tag{7}$$

where t_1, t_2, and t_3 are the unit vector components of the rotation axis $\mathbf{t}$. The $\boldsymbol{\sigma}_{\mathrm{applied}}$ was chosen such that RSS = 1 on the slip plane of IN grain for both {110} and {112} cases. That is, if Eq. (6) had $\boldsymbol{n}_{\mathbf{in}}$ and $\boldsymbol{b}_{\mathbf{in}}$, then the RSS = 1 for both {110} and {112} slip plane cases. To calculate these parameters for a given GB configuration, the slip system in the IN grain was fixed and the

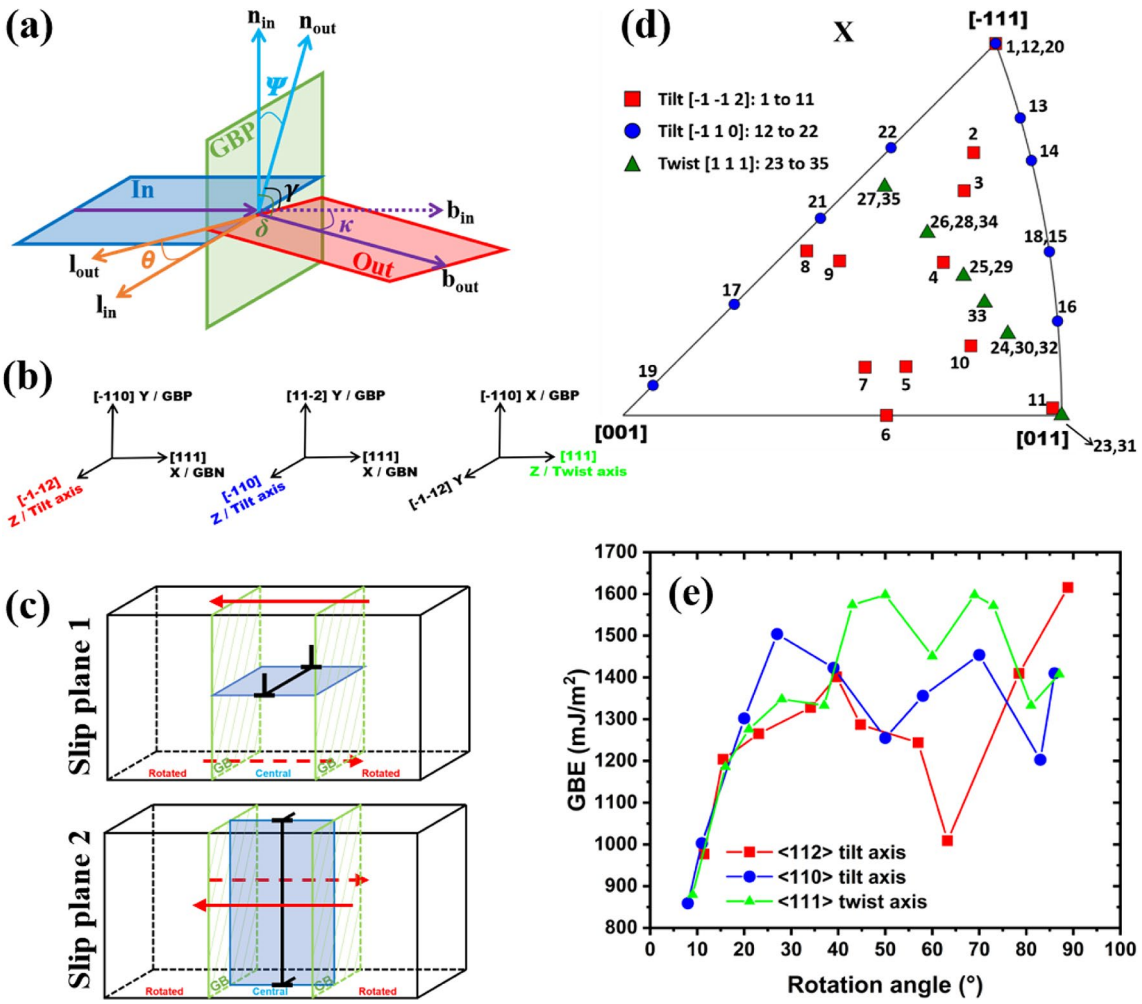

Figure 1 **a** Schematic illustration of slip transmission from IN grain to OUT grain through GBP. The slip plane in the IN grain containing the dislocation is shown in blue color and the possible slip plane of the rotated OUT grain is shown in red color. By the slip transmission theory, the misorientation between the OUT and IN grains can be by any arbitrary rotation axis and rotation angle. The GBP between two differently oriented grains is shown in green color. $\boldsymbol{n}_{in}$ and $\boldsymbol{n}_{out}$ are the slip plane normals of the incoming and outgoing dislocations, respectively. $\boldsymbol{b}_{in}$ and $\boldsymbol{b}_{out}$ are the Burger vectors of incoming and outgoing dislocations, respectively. $\boldsymbol{l}_{in}$ and $\boldsymbol{l}_{out}$ are dislocation line directions of the incoming and outgoing dislocations, respectively. The angle between $\boldsymbol{n}_{in}$ and $\boldsymbol{n}_{out}$ is Ψ, between $\boldsymbol{b}_{in}$ and $\boldsymbol{b}_{out}$ is κ, between $\boldsymbol{l}_{in}$ and $\boldsymbol{l}_{out}$ is θ, between $\boldsymbol{b}_{in}$ and $\boldsymbol{n}_{out}$ is γ, and between $\boldsymbol{b}_{out}$ and $\boldsymbol{n}_{in}$ is δ. **b** Coordinate axes and directions for three rotation axes. **c** Schematic illustrations of GB configurations with dislocation on two different slip planes for a given rotation axis. For $[\bar{1}\ \bar{1}2]$ and [111] rotation axes, slip plane 1 represent {110} and slip plane 2 represent {112} while for $[\bar{1}10]$ rotation axis slip plane 1 represent {112} and slip plane 2 represent {110}. The arrows represent the shear direction. **d** Orientations along X direction shown on a standard triangle of the stereographic projection. The red colored symbols represent $[\bar{1}\ \bar{1}2]$ tilt GB configurations, the blue colored symbols represent $[\bar{1}10]$ tilt GB configurations, and the green colored symbols represent [111] twist GB configurations. The central grain in each of the GB configurations ($[\bar{1}\ \bar{1}2]$ tilt, $[\bar{1}10]$ tilt, [111] twist) are 1, 12, and 23, respectively. The orientation of the other numberings is referred in Table s1 in the supplementary file. **e** GBE as a function of the rotation angle

script containing the code stabix [31] and the program MTEX [32] was run for all the possible 48 slip systems in the rotated OUT grain to obtain STP. As the script looped over every slip system, the vectors $\boldsymbol{n}_{out}$, $\boldsymbol{b}_{out}$, and $\boldsymbol{l}_{out}$ changed accordingly.

Residual burger vector (RBV) is the magnitude of the difference between $\boldsymbol{b}_{in}$ and $\boldsymbol{b}_{out}$ as,

$$\text{RBV} = |\boldsymbol{b}_r| = |\boldsymbol{b}_{\text{in}} - \boldsymbol{b}_{\text{out}}| = |\boldsymbol{b}_{\text{in}} - \boldsymbol{R}\boldsymbol{b}_{\text{in}}|, \quad (8)$$

where $\boldsymbol{b}_{\text{out}}$ was calculated directly by $\boldsymbol{b}_{\text{out}} = \boldsymbol{R}\boldsymbol{b}_{\text{in}}$. For slip transmission to occur m', N, LRB, λ, s, and RSS should be maximum, while RBV should be minimum.

Molecular dynamics simulations

The transmission of dislocations through various GBs was also simulated using molecular dynamics. The asymmetric tilt/twist GB configurations were modeled with $[\bar{1}\ \bar{1}2]$ and $[\bar{1}10]$ as tilt axes and [111] as twist axis (Fig. 1b). The central grain (similar to IN grain in "Slip transmission parameters" section) was fixed to enable the slip of an edge dislocation on either {110} or {112} slip planes and the neighboring grains were rotated about either $[\bar{1}\ \bar{1}2]/[\bar{1}10]/[111]$ between 0° and 90°. Thus, with 32 different GB configurations and 2 slip planes, 64 MD simulations were carried out. The orientation of the rotated grains is shown in Fig. 1d. The two rotated grains on either side of the central grain had similar orientations/rotations and the grain's dimensions were equal to the integer multiple of the magnitude of the direction vectors to obtain periodic boundaries along GB normal (GBN) and GB plane (GBP). The central grain was translated along GBP and equilibrated using conjugate gradient method to arrive at the lowest energy configuration. The GB energy (GBE) was calculated as the excess of cohesive energy due to the GB [33, 34]. The GBE as a function of rotation angle is shown in Fig. 1e and the values are tabulated in Table s1. Atomsk [35] was used to insert an edge dislocation by adding an extra plane of atoms along $\langle 110 \rangle$ in the central grain. The configurations were sheared by altering the simulation box with a shear strain of 10^{-5} along [111] and equilibrated using conjugate gradient method [36]. The direction [111] was selected as the shear direction as it is the slip direction for the dislocation in bcc system. All simulations were carried out with a system temperature of 0 K using an interatomic potential developed by Chen et al. [37]. The system temperature of 0 K was chosen to exclude any effect due to thermal fluctuations. The choice of this potential was made after checking the lattice constant, cohesive energy, elastic constants and core structure of screw dislocation in bulk Ta predicted by the potential with that of the experimental and first principles data. The configurations were referred to by the notation $\langle rotation\_axis \rangle / \theta° / \{slip\_plane\}$ representing the rotation axis, rotation angle, and slip plane. Simulations were run using LAMMPS [38] and visualized using OVITO [39].

Machine learning models

Machine learning was used to correlate the STPs and MD parameters to the stress at which the GB either absorbs or transmits the incoming dislocation, called as yield stress of the GB. To do this, the slip transmission and MD parameters were taken as input 'features' and yield of the GB was taken as output target for ML models—XGBoost (version 1.7.6) and SHAP. The pre-processing step involved feature engineering in which a Pearson correlation plot was used to find the dependence between the features so as to decide on the features to use during ML. Randomly selected 75% of the data was used for training and the remaining 25% for testing. XGBoost minimizes the objective function

$$\text{obj} = \left[\sum_{i=1}^{K} L\left(y_i, p_i^0 + O_{\text{value}}\right)\right] + \gamma T + \frac{1}{2}\lambda_{\text{ML}} O_{\text{value}}^2 \quad (9)$$

to predict the output value O_{value} using gradient-boosted trees [27]. The first term of Eq. (9) is the summation of the loss function L for K number of observations in the training data [40]. L is a function of the observed output target values from MD simulations y_i, the initially predicted value p_i^0 which is usually taken as 0.5, and the predicted output value O_{value}. γ is for pruning and T is the number of terminal nodes in a tree. The last term is the regularization term with the regularization parameter λ_{ML}. The XGBoost hyperparameters were optimized to arrive at the lowest root mean square error (RMSE) possible calculated as, $\text{RMSE} = \sqrt{\frac{\sum_{t=1}^{M}(y_t - O_{\text{value}})^2}{M}}$, where M is the number of observations in the test data. The explanation of the XGBoost model f was carried out using SHAP. SHAP trains the model on each feature subset S taken from the set of all features F. The importance of each feature is calculated by training the model with the feature $f_{S\cup\{j\}}\left(x_{S\cup\{j\}}\right)$ and without the feature $f_S(x_S)$ where x is the value of the input feature. The SHAP value of a feature is calculated as,

$$\phi_j = \sum_{S\subseteq F} \frac{|S|!(|F| - |S| - 1)!}{|F|!}\left[f_{S\cup\{j\}}\left(x_{S\cup\{j\}}\right) - f_S(x_S)\right]. \quad (10)$$

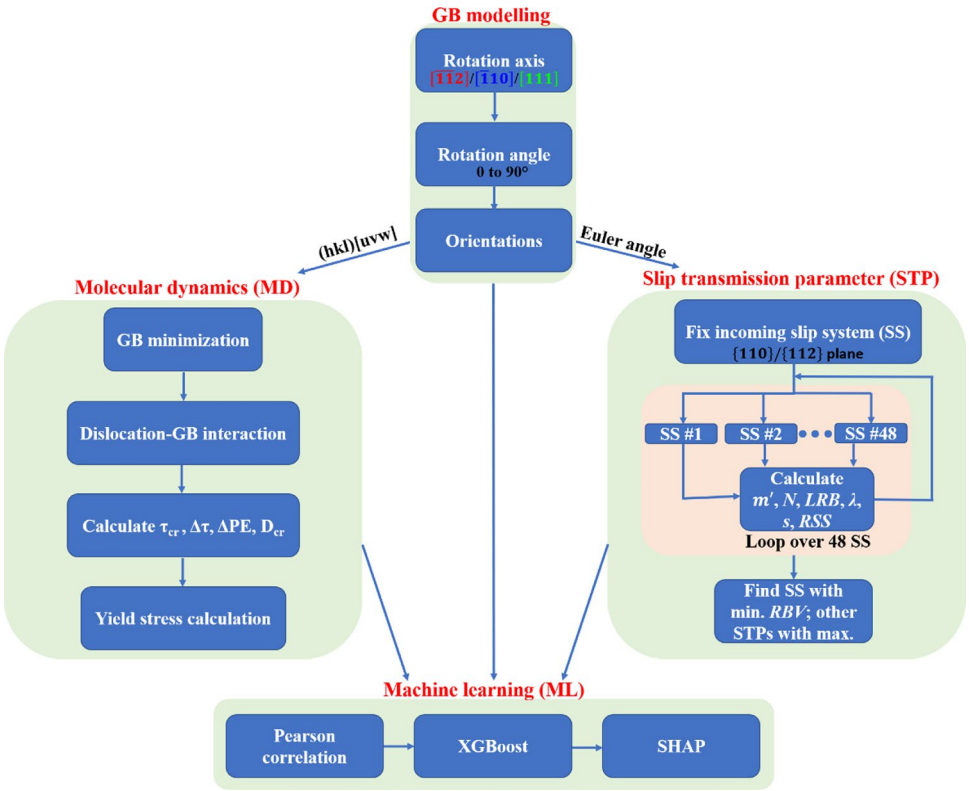

Figure 2 Schematic flowchart of the work carried out in this article. MD parameters τ_{cr}, $\Delta\tau$, ΔPE, and D_{cr} are discussed in Sect. "Molecular dynamics simulations"

All data were used for SHAP analysis. The data and scripts for numerical calculation, MD, and ML are available in the GitHub link. The schematic flowchart of the work carried out is shown in Fig. 2.

Results and discussion

Slip transmission parameters

The main observations from Fig. 3 were as follows. First, m', LRB, and RSS (i.e., Eqs. 1,3, and 6) did not show sensitivity to [111] twist GB configurations. The prediction of slip transmission in twist GB configurations is of importance because the orientations in twist GB configurations correspond to the orientations of γ fiber in bcc which are formed during plastic deformation [41, 42]. Further, RBV and LRB could not differentiate between dislocations on {110} or {112} slip planes, but experimental and simulation results have shown that {110}⟨111⟩ and {112}⟨111⟩ slip systems have different CRSS values [43].

Molecular dynamics simulations

The slip transmission through GB can be visualized as a three-stage process of pile-up, absorption, and transmission. The pile-up of dislocations was observed in ⟨112⟩/16°/{110}, ⟨110⟩/8°/{112}, and ⟨110⟩/11°/{112}. Partial pile-up similar to a disconnection formation in the GB surface was observed in ⟨110⟩/86°/{112} and ⟨111⟩/81°/{110}. Absorption followed by transmission was observed in ⟨112⟩/11°/{110}, ⟨112⟩/11°/{112}, ⟨112⟩/16°/{112}, ⟨110⟩/8°/{110}, ⟨110⟩/11°/{110}, ⟨110⟩/70°/{112}, ⟨111⟩/8°/{110}, ⟨111⟩/16°/{110}, ⟨111⟩/8°/{112}, ⟨111⟩/16°/{112}, and ⟨111⟩/60°/{112}. The interaction of dislocation with the LAGB showed the formation of dislocation networks during pinning and looping. The snapshots of configurations in which dislocations in the GB were visible are shown in Fig. 4 and their videos are attached as supplementary file.

The dislocation–GB interactions using MD simulations were quantified using parameters such as critical shear stress for absorption of dislocation by the GB (τ_{cr} in MPa), drop in shear stress ($\Delta\tau$ in MPa), drop

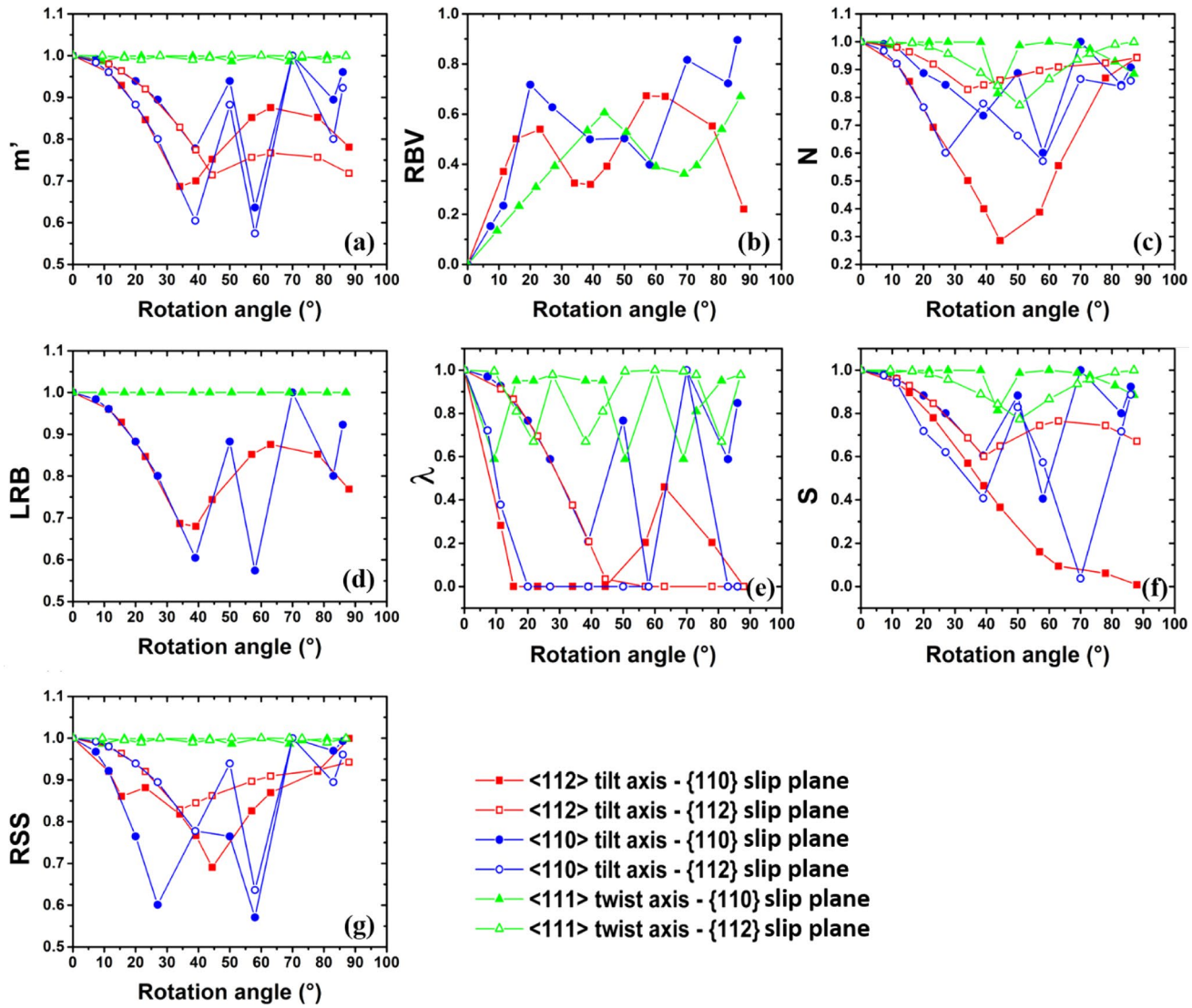

Figure 3 Slip transmission parameters calculated with orientations of the rotated grains for various GB configurations

in potential energy (ΔPE in eV), and critical distance between the dislocation and GB just before the absorption of a dislocation (D_{cr} in nm). These were recorded at the event of dislocation absorption or piling-up near the GB as shown in Figs. S1 and S2 in the supplementary file. Figure 5a shows that τ_{cr} was high for $[\bar{1}\bar{1}2]$ tilt axis configurations with {110} slip being dominant. According to the dislocation pile-up model [25, 44, 45], the shear stress reaches a critical value τ_y when the dislocation gets either absorbed by or transmitted through the GB and is expressed as,

$$\tau_y = \tau_o + \sqrt{\frac{\tau_{cr} T}{Lb}} \tag{11}$$

where $T = \overline{\alpha} Gb^2$, and the distance between the source and GB is $L = d/2$ with d being the GB spacing. Hence,

$$\tau_y = \tau_o + \sqrt{\frac{2\tau_{cr}\overline{\alpha} Gb}{d}}. \tag{12}$$

The yield stress (σ_y) and shear stress at yield of the GB configuration τ_y are related through a constant A as,

$$\sigma_y = A\tau_y = A\tau_o + A\sqrt{\frac{2\tau_{cr}\overline{\alpha} Gb}{d}} = \sigma_o + \frac{k_{HP}}{\sqrt{d}} \tag{13}$$

where the Hall–Petch constant is $k_{HP} = A\sqrt{2\tau_{cr}\overline{\alpha} Gb}$. For pure Ta, $\overline{\alpha} \approx 1$, $G = 69$ GPa, $b = 0.2863$ nm, and σ_o

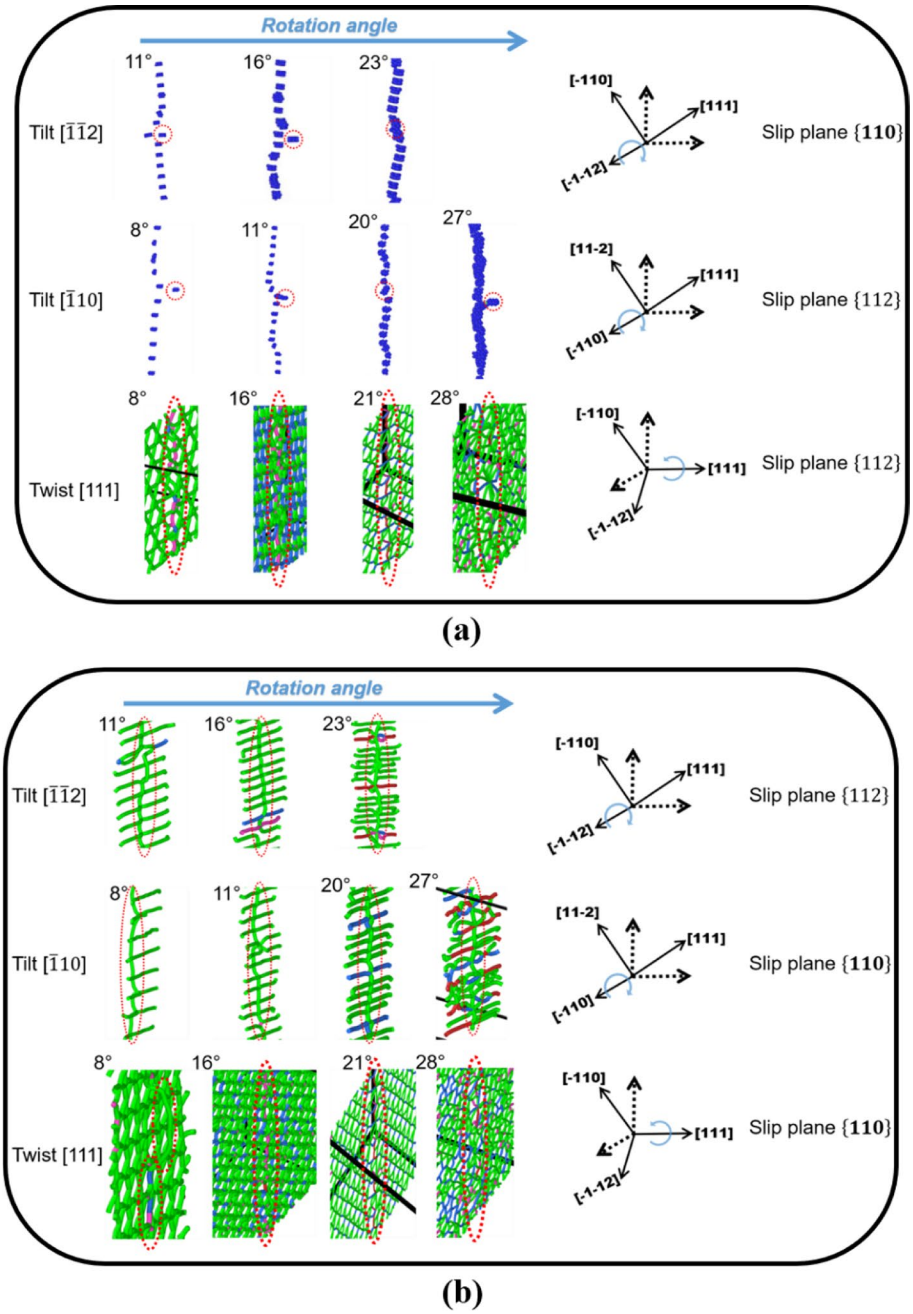

Figure 4 MD snapshots of dislocation interaction with GB configurations which had dislocations. The dislocations with Burgers vector type ⟨111⟩ are colored green, ⟨110⟩ are colored blue, ⟨100⟩ are colored pink, other types are colored red. The GB configurations which are difficult to visualize using the above are shown using atoms only whose neighbors are not equal to eight. Atoms with eight neighbors are removed for better visualization. The incoming dislocation is shown using dotted red colored oval/circle. **a** Interactions of parallel dislocations while **b** interactions of perpendicular dislocations where one dislocation is the incoming and other is in the GB. This is independent for twist GB configurations

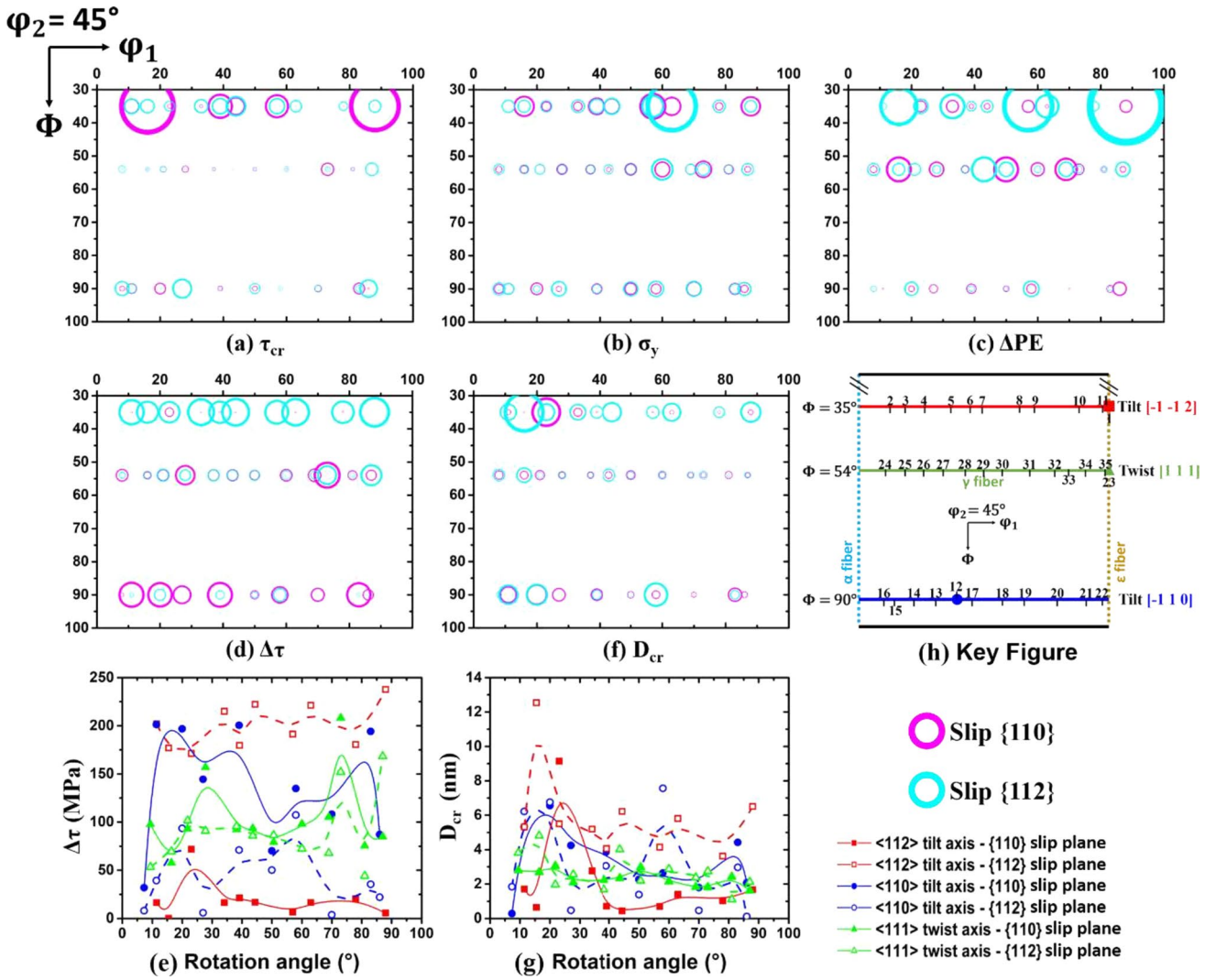

Figure 5 The values of the parameters calculated from MD simulations are represented as circles with the orientation of the rotated grain for various GB configurations as the location on the Euler space. The pink open circles represent {110} slip plane and the cyan open circles represent {112} slip plane for **a**–**d** and **f**. The size/radius of the circle is proportional to the values of the MD parameters but the scaling factor is different between the parameters. The key figure for 5a-5d and 5f is shown in 5 h. The orientations of the central grains for each rotation axis are shown as symbols in the key figure. The orientations of the rotated grains (numbering as in Table s1) lie on the lines represented by various colors and rotation axes. The value of φ_1 lies between 0° and 90° as orthotropic symmetry was assumed. And also, for ease of representation of $[\bar{1}\ \bar{1}2]$ and $[\bar{1}10]$ tilt GB configurations, φ_2 of these two configurations are shifted from 225° and 315° to 45°. Figures 5e and 5 g represent the variation of drop in shear stress and critical distance as a function of rotation angle connected by the b-spline curve

= 80 MPa. The value of $A = 7$ is chosen so as to get a value of $k_{HP} = 476\text{MPa}\sqrt{\mu\text{m}}$ close to that found in the literature [42].

The stored energy due to the GB (E) per molar volume (V) of Ta for rotation angle θ is [46],

$$\frac{E}{V} = \frac{K\theta\gamma_m}{d\theta_m}\left[1 - \ln\left(\frac{\theta}{\theta_m}\right)\right]. \tag{14}$$

where $K = 3.31$, $\gamma_m = 966\text{mJ/m}^2$, and $\theta_m = 23°$ [46]. The stored energy can be substituted by the GBE (E_{gb}) occupying a unit meter squared area of A_{gb}, thus Eq. (14) becomes,

$$\frac{E_{gb}A_{gb}}{V} = \frac{K\theta\gamma_m}{d\theta_m}\left[1 - ln\left(\frac{\theta}{\theta_m}\right)\right]. \quad (15)$$

Rearranging Eq. (15) gives

$$d = \frac{VK\theta\gamma_m}{E_{gb}\theta_m}\left[1 - ln\left(\frac{\theta}{\theta_m}\right)\right]. \quad (16)$$

Substituting the expression of d in Eq. (13) gives

$$\sigma_y = \sigma_o + A\sqrt{\frac{2\tau_{cr}GbE_{gb}\theta_m}{VK\theta\gamma_m\left[1 - ln\left(\frac{\theta}{\theta_m}\right)\right]}}. \quad (17)$$

For pure Ta, $V = 10.85 \times 10^{-6}\text{m}^3\text{mol}^{-1}$. Taking τ_{cr}, E_{gb}, and their corresponding θ from MD simulation results, the mean value of σ_y was found to be 206 MPa which corresponds to the yield strength of coarse-grained Ta [42]. Negligible variation in σ_y between slip planes was observed except in case of ⟨112⟩/63°/{112} as in Fig. 5b.

During the initial deformation, the increase in the PE and shear stress τ corresponds to the energy and stress accumulation, respectively. The sudden drop in PE and τ corresponds to the absorption of the dislocation by the GB. GBs act as sinks for dislocations that results in a reduction in the strain energy. As the strain energy of an edge dislocation is constant in the present cases, the significance of ΔPE and $\Delta\tau$ can be correlated to the energy and stress relaxation of the GB, respectively, during the absorption event. ⟨112⟩/{112} showed a significant ΔPE and $\Delta\tau$ as in Fig. 5c, d. Figure 5e has similarities to that of N and s in Figs. 3c, f; for example, the variation of values in ⟨112⟩/{110} was lower than ⟨112⟩/{112}

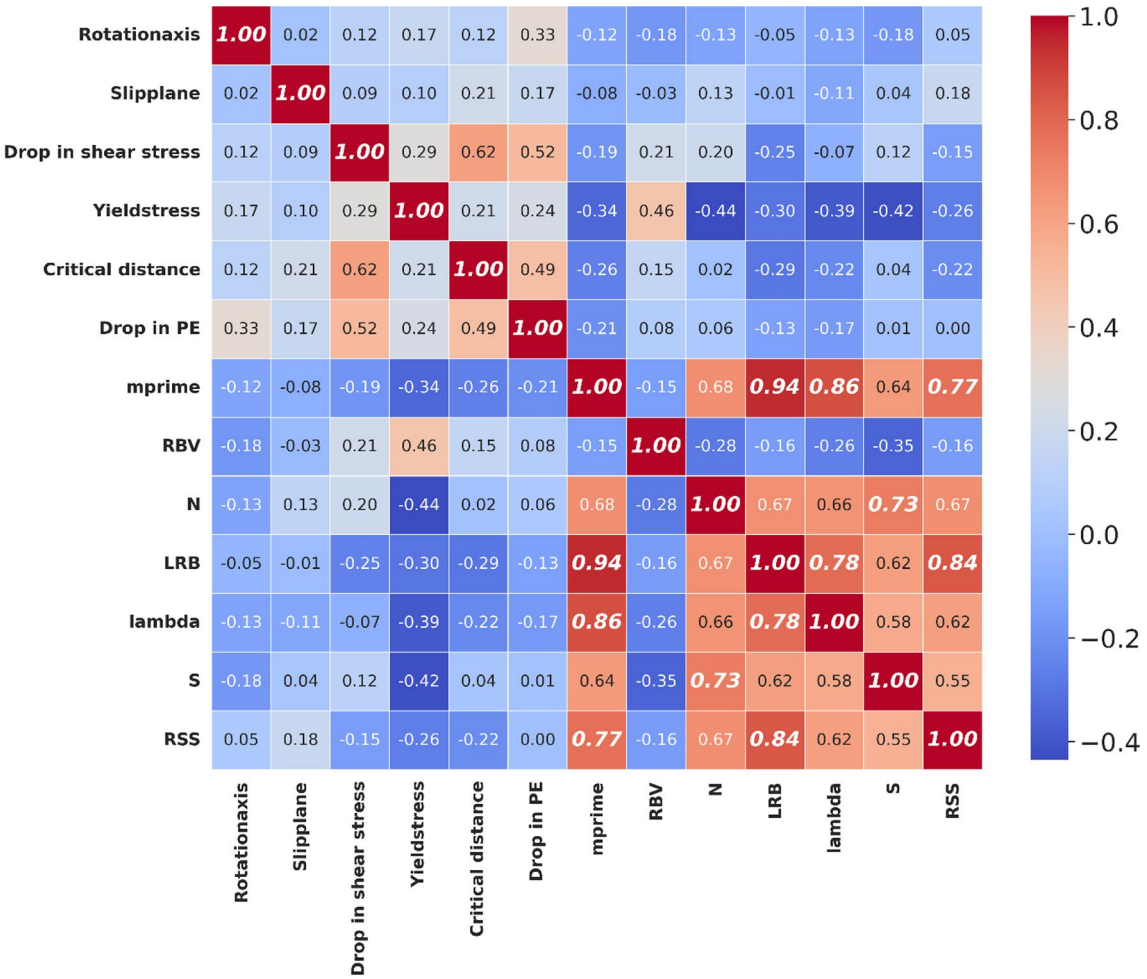

Figure 6 Pearson correlation plot between various features. The values of the features showing strong correlation (here, greater than 0.7) are shown as bold text

while ⟨110⟩/{110} was higher than ⟨110⟩/{112}. D_{cr} is dependent on the extent of attraction of the dislocation to the GB. D_{cr} increased with initial values of rotation angles for LAGBs and then decreased for higher values of rotation angles as in Figs. 5f, g.

Feature analysis using SHAP

Using the Pearson correlation plot in Fig. 6, only the least correlated features were used as inputs while other features with correlation coefficient greater than 0.7 such as N, LRB, λ, and RSS were not used. The outliers belonging to ⟨112⟩/15°/{110}, ⟨112⟩/88°/{110}, and ⟨112⟩/63°/{112} were removed due to the higher shear stress values.

The rotation axis and slip plane along with MD parameters $\Delta\tau$, ΔPE and D_{cr}; and the STPs m', RBV, and s were taken as input features. The yield stress calculated from Eq. (17) was the output target. The other MD parameters such as τ_{cr}, E_{gb}, and rotation angle were neglected as they were already correlated to the yield stress by Eq. (17).

The XGBoost hyperparameters used in the current model were max depth, gamma, colsample bytree, sub-sample, learning rate, max delta step, random state, n estimators, alpha, and seed. To avoid local optima, surrogate model with any two hyperparameters were optimized using grid search and the other hyperparameters were fixed to their default or initial seed values. The surrogate model was again used with another two hyperparameters being optimized using grid search. This process was repeated using other hyperparameters to arrive at the final optimized XGBoost model. This method was used to save computational time and cost. The XGBoost hyperparameters were optimized until RMSE between the XGBoost predicted and calculated yield stress during testing was as low as possible, here 37 MPa. RMSE during testing was 37 MPa while RMSE during training was 12 MPa ensuring that there was no overfitting. The optimized values of XGBoost hyperparameters are shown in Table 1. The cross-validation of the optimized model was carried out with 5 splits and their RMSEs were 112, 109, 125, 49, and 63 MPa. The average RMSE across data was 92 MPa with a standard deviation of 29 MPa.

Table 1 Optimized XGBoost hyperparameters

XGBoost hyperparameters	Values
Max depth	3
Gamma	85
Colsample bytree	0.191421
Subsample	0.284894
Learning rate	0.843006
Max delta step	67
Random state	1
n estimators	99
Alpha	6
Seed	19

The ML predicted values matched reasonably well with the MD calculated values of the yield stress (Fig. 7a). The sorted feature with decreasing mean SHAP values in Fig. 7b is a quantitative dependence on yield stress. The features D_{cr}, $\Delta\tau$ and m' showed maximum correlation with yield stress. m' was found to contribute significantly to the yield stress as compared to any other STP. The low/high feature value and its corresponding negative/positive SHAP value represent direct proportionality between the feature and the yield stress. Whereas a low/high feature value and its corresponding positive/negative SHAP value represents inverse proportionality between the feature and the yield stress. For example, an increase in $\Delta\tau$, or a decrease in D_{cr} or m' corresponds to an increase the yield stress which can be attributed to strengthening of GBs. That is, if a GB configuration **A** has higher $\Delta\tau$ or lower D_{cr}/m' than that of **B** GB configuration, then **A** is stronger than **B**. When D_{cr} was less than 40 Å, there was a stronger contribution toward increase of the yield stress as in Fig. 7c. So, the GB configurations that resulted in D_{cr} being less than 40 Å were stronger than those with D_{cr} greater than 40 Å. There were 44 GB configurations with D_{cr} less than 40 Å. The complete data is available in the GitHub link. A high value of $\Delta\tau$ was due to the large relaxation (during dislocation absorption) of strained GB, which can be attributed to the higher strength of the GB configuration and hence an increase in yield stress. So, the GB configurations with the value of $\Delta\tau$ between 15 and 70 MPa and SHAP values less than zero were weaker than that with SHAP values greater than zero as in Fig. 7d. {110} slip plane had negative SHAP values indicating it would decrease the yield stress while {112} would increase the yield stress (Fig. 7e). This implied that the configurations with dislocation on {110} were weaker than that with dislocation on {112} slip plane. [111] rotation axis showed higher SHAP values as in Fig. 7f. This implied that microstructures

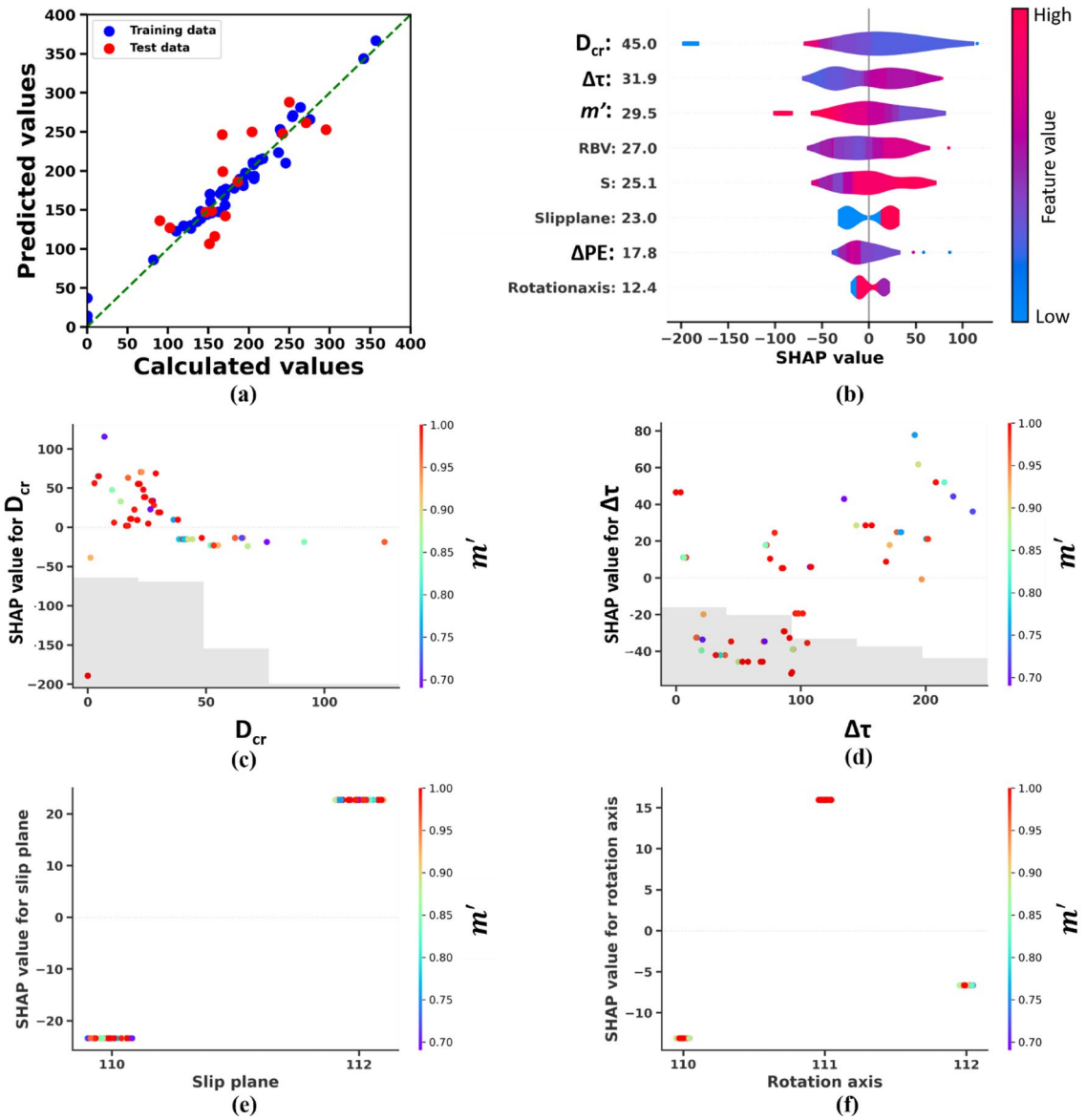

Figure 7 **a** MD calculated and XGBoost predicted yield stress values for both the training and testing data. **b** SHAP violin plot for all features. SHAP values are in the units of log-odds. The maximum and minimum value of the feature is represented on a color bar on the right side of **b**. SHAP dependence plot of **c** critical distance and **d** drop in shear stress. The histogram shows the distribution of number of data points. SHAP dependence plot of **e** slip plane and **f** rotation axis. The points in Figs. **c**–**f** were colored using values of m'

with continuous grains of γ fiber will be difficult to deform due to their [111] rotation axis configurations.

Conclusions

Dislocation–GB interaction plays a critical role in governing the plastic deformation of a material. Slip transmission across the GBs during plastic deformation is a complex process and is determined by several factors. The orientations and types of GBs studied in the present work are a small subset of the total possibilities. Even with these limitations, the results obtained from the study helped to an extent in solving the ambiguity of the slip transmission parameters and gave a path to relate these parameters with the yield strength relating to deformation of GB. The results were also helpful in distinguishing the effect of GB configurations

with different rotation axes and slip planes on the yield stress. The MD simulation results can be useful in crystal plasticity simulations where dislocation–GB interactions require atomistic inputs.

The main conclusions are listed below.

1. Numerical calculations of STPs revealed that m', LRB, and RSS could not explain the slip transmission through [111] twist GB configurations. RBV and LRB could not distinguish between dislocation slipping on {110} and {112} planes. N, LRB, λ, and RSS were not considered for ML analysis as they showed a strong correlation with other parameters.
2. The yield stress of the GB configurations were estimated using GB properties such as GBE, rotation angle, τ_{cr}, and their mean value was found to be 206 MPa.
3. XGBoost and SHAP were used to explain the correlation of various STPs and MD parameters with yield stress. The yield stress can be best quantified using D_{cr}, $\Delta\tau$ and m'. The configurations with D_{cr} less than 40 Å and with higher $\Delta\tau$ values were difficult to deform relative to other configurations. The SHAP results sorted the prominent slip plane and rotation axis affecting the yield stress. Dislocations on {110} slip plane could yield the GB relatively easy (negative SHAP value) as compared to those on {112} (positive SHAP value). The yield stress was highest for GB configurations with rotation axis [111], followed by $[\bar{1}\bar{1}2]$ and $[\bar{1}10]$.

Quantifying the dislocation transmission through a GB via slip is essential in predicting the strength of materials and has till now been done through slip transmission parameters. Our work presents a novel methodology of integrating the slip transmission parameters and parameters from molecular dynamics simulations, using explainable machine learning to bring out the specific parameters that correlate well with the yield of the GB. The use of machine learning toward solving this essential scientific problem opens a new avenue revolutionizing the slip transmission theory.

Data and code availability

The data that support the findings of this study are openly available in Github, at https://github.com/kedhar1992/dislocation-GB.

Acknowledgements

This work was supported under the BARC project RBA4012 'Development of new generation alloys for nuclear reactor system and joining technologies for ceramics, metals and special materials'.

Author contributions

AK contributed to conceptualization, methodology, simulation, data collection, analysis, evaluation, and writing of the original manuscript. RK contributed to supervision, critical discussion, review, and editing of the manuscript. AS contributed to simulation, critical discussion, review, and editing of the manuscript.

Declarations

Conflict of interest The authors declare that they have no known competing financial interests or personal relationships that could have appeared to influence the work reported in this paper.

Ethical approval Not applicable.

Supplementary Information The online version contains supplementary material available at https://doi.org/10.1007/s10853-023-09167-y.

References

[1] Hansen N (2004) Hall-petch relation and boundary strengthening. Scr Mater 51:801–806. https://doi.org/10.1016/j.scriptamat.2004.06.002

[2] Patriarca L, Abuzaid W, Sehitoglu H, Maier HJ (2013) Slip transmission in bcc FeCr polycrystal. Mater Sci Eng A 588:308–317. https://doi.org/10.1016/j.msea.2013.08.050

[3] Guo Y, Britton TB, Wilkinson AJ (2014) Slip band-grain boundary interactions in commercial-purity titanium. Acta Mater 76:1–12. https://doi.org/10.1016/j.actamat.2014.05.015

[4] Bieler TR, Eisenlohr P, Zhang C, Phukan HJ, Crimp MA (2014) Grain boundaries and interfaces in slip transfer. Curr Opin Solid State Mater Sci 18:212–226. https://doi.org/10.1016/j.cossms.2014.05.003

[5] Weaver JS, Li N, Mara NA, Jones DR, Cho H, Bronkhorst CA, Fensin SJ, Gray GT (2018) Slip transmission of high angle grain boundaries in body-centered cubic metals: micropillar compression of pure Ta single and bi-crystals. Acta Mater 156:356–368. https://doi.org/10.1016/j.actamat.2018.06.046

[6] Kondo S, Mitsuma T, Shibata N, Ikuhara Y (2016) Direct observation of individual dislocation interaction processes with grain boundaries, Science. Advances 2:1–8. https://doi.org/10.1126/sciadv.1501926

[7] Shen Z, Wagoner RH, Clark WAT (1988) Dislocation and grain boundary interactions in metals. Acta Metall 36:3231–3242. https://doi.org/10.1016/0001-6160(88)90058-2

[8] De Koning M, Kurtz RJ, Bulatov VV, Henager CH, Hoagland RG, Cai W, Nomura M (2003) Modeling of dislocation-grain boundary interactions in FCC metals. J Nucl Mater 323:281–289. https://doi.org/10.1016/j.jnucmat.2003.08.008

[9] Shimokawa T, Kinari T, Shintaku S (2007) Interaction mechanism between edge dislocations and asymmetrical tilt grain boundaries investigated via quasicontinuum simulations. Phys Rev B 75:1–11. https://doi.org/10.1103/PhysRevB.75.144108

[10] Yu W, Wang Z (2012) Interactions between edge lattice dislocations and Σ11 symmetrical tilt grain boundaries in copper: a quasi-continuum method study. Acta Mater 60:5010–5021. https://doi.org/10.1016/j.actamat.2012.06.037

[11] Wang J (2015) Atomistic simulations of dislocation pileup: grain boundaries interaction. Jom 67:1515–1525. https://doi.org/10.1007/s11837-015-1454-0

[12] Liang Y, Yang X, Gong M, Liu G, Liu Q, Wang J (2019) Interactions between dislocations and three-dimensional annealing twins in face centered cubic metals. Comput Mater Sci 161:371–378. https://doi.org/10.1016/j.commatsci.2019.02.024

[13] Chandra S, Samal MK, Chavan VM, Patel RJ (2015) Atomistic simulations of interaction of edge dislocation with twist grain boundaries in Al-effect of temperature and boundary misorientation. Mater Sci Eng A 646:25–32. https://doi.org/10.1016/j.msea.2015.08.049

[14] Kacher J, Eftink BP, Cui B, Robertson IM (2014) Dislocation interactions with grain boundaries. Curr Opin Solid State Mater Sci 18:227–243. https://doi.org/10.1016/j.cossms.2014.05.004

[15] Kacher J, Robertson IM (2014) In situ and tomographic analysis of dislocation/grain boundary interactions in titanium. Philos Mag 94:814–829. https://doi.org/10.1080/14786435.2013.868942

[16] Hansen LT, Fullwood DT, Homer ER, Wagoner RH, Lim H, Carroll JD, Zhou G, Bong HJ (2020) An investigation of geometrically necessary dislocations and back stress in large grained tantalum via EBSD and CPFEM. Mater Sci Eng, A 772:138704. https://doi.org/10.1016/j.msea.2019.138704

[17] Bayerschen E, McBride AT, Reddy BD, Böhlke T (2016) Review on slip transmission criteria in experiments and crystal plasticity models. J Mater Sci 51:2243–2258. https://doi.org/10.1007/s10853-015-9553-4

[18] Ren Y, Huang Z, Wang Y, Zhou Q, Yang T, Li Q, Jia Q, Wang H (2023) Friction-induced rapid amorphization in a wear-resistant (CoCrNi)88Mo12 dual-phase medium-entropy alloy at cryogenic temperature. Compos B Eng 263:110833. https://doi.org/10.1016/j.compositesb.2023.110833

[19] Mortazavi B, Silani M, Podryabinkin EV, Rabczuk T, Zhuang X, Shapeev AV (2021) First-principles multiscale modeling of mechanical properties in graphene/borophene heterostructures empowered by machine-learning interatomic potentials. Adv Mater. https://doi.org/10.1002/adma.202102807

[20] Zhou Q, Luo D, Hua D, Ye W, Li S, Zou Q, Chen Z, Wang H (2022) Design and characterization of metallic glass/graphene multilayer with excellent nanowear properties. Friction 10:1913–1926. https://doi.org/10.1007/s40544-021-0581-6

[21] Yang C, Yin C, Wu Y, Zhou Q, Liu X (2023) Atomic insights into the deformation mechanism of an amorphous wrapped nanolamellar heterostructure and its effect on self-lubrication. J Market Res 26:4206–4218. https://doi.org/10.1016/j.jmrt.2023.08.215

[22] Talebi H, Silani M, Bordas SPA, Kerfriden P, Rabczuk T (2014) A computational library for multiscale modeling of material failure. Comput Mech 53:1047–1071. https://doi.org/10.1007/s00466-013-0948-2

[23] Spearot DE, Sangid MD (2014) Insights on slip transmission at grain boundaries from atomistic simulations. Curr Opin Solid State Mater Sci 18:188–195. https://doi.org/10.1016/j.cossms.2014.04.001

[24] Tsuru T, Shibutani Y, Hirouchi T (2016) A predictive model for transferability of plastic deformation through grain boundaries. AIP Adv. https://doi.org/10.1063/1.4939819

[25] Kapoor R, Verdhan N (2017) Interaction of dislocation pile-up with a low-angle tilt boundary: a discrete dislocation dynamics study. Philos Mag 97:465–488. https://doi.org/10.1080/14786435.2016.1266102

[26] Kedharnath A, Kapoor R, Sarkar A (2021) Classical molecular dynamics simulations of the deformation of metals under uniaxial monotonic loading: a review. Comput Struct 254:106614. https://doi.org/10.1016/j.compstruc.2021.106614

[27] Chen T, Guestrin C (2016) XGBoost: A scalable tree boosting system. In: Proceedings of the ACM SIGKDD international conference on knowledge discovery and data mining. ACM, New York, NY, USA, pp 785–794. https://doi.org/10.1145/2939672.2939785

[28] Lundberg SM, Lee SI (2017) A unified approach to interpreting model predictions. Adv Neural Inf Process Syst 30:4766–4775

[29] Werner E, Prantl W (1990) Slip transfer across grain and phase boundaries. Acta Metall Mater 38:533–537. https://doi.org/10.1016/0956-7151(90)90159-E

[30] Priester L, Boundaries G (1976). From Theory to Engineering. https://doi.org/10.1017/cbo9781316389508.016

[31] Mercier D, Zambaldi C, Bieler TR (2015) A Matlab toolbox to analyze slip transfer through grain boundaries. IOP Conf Ser Mater Sci Eng 82:11–15. https://doi.org/10.1088/1757-899X/82/1/012090

[32] Mainprice D, Bachmann F, Hielscher R, Schaeben H (2015) Descriptive tools for the analysis of texture projects with large datasets using MTEX: strength, symmetry and components. Geol Soc Spec Pub 409:251–271. https://doi.org/10.1144/SP409.8

[33] Kedharnath A, Kapoor R, Sarkar A (2019) Atomistic simulation of interaction of collision cascade with different types of grain boundaries in α-Fe. J Nucl Mater 523:444–457. https://doi.org/10.1016/j.jnucmat.2019.06.021

[34] Kedharnath A, Panwar AS, Kapoor R (2017) Molecular dynamics simulation of the interaction of a nano-scale crack with grain boundaries in α-Fe. Comput Mater Sci 137:85–99. https://doi.org/10.1016/j.commatsci.2017.05.026

[35] Hirel P (2015) Atomsk: a tool for manipulating and converting atomic data files. Comput Phys Commun 197:212–219. https://doi.org/10.1016/j.cpc.2015.07.012

[36] W.R. Jian, S. Xu, I.J. Beyerlein, On the significance of model design in atomistic calculations of the Peierls stress in Nb, Computational Materials Science. 188 (2021). https://doi.org/10.1016/j.commatsci.2020.110150.

[37] Chen Y, Fang J, Liu L, Hu W, Gao N, Gao F, Deng H (2019) Development of the interatomic potentials for W-Ta system. Comput Mater Sci 163:91–99. https://doi.org/10.1016/j.commatsci.2019.03.021

[38] Plimpton S (1995) Fast parallel algorithms for short-range molecular dynamics. J Comput Phys 117:1–19. https://doi.org/10.1006/jcph.1995.1039

[39] Stukowski A (2010) Visualization and analysis of atomistic simulation data with OVITO-the open visualization Tool. Modell Simul Mater Sci Eng 18:015012. https://doi.org/10.1088/0965-0393/18/1/015012

[40] Samaniego E, Anitescu C, Goswami S, Nguyen-Thanh VM, Guo H, Hamdia K, Zhuang X, Rabczuk T (2020) An energy approach to the solution of partial differential equations in computational mechanics via machine learning: Concepts, implementation and applications. Comput Methods Appl Mech Eng 362:112790. https://doi.org/10.1016/j.cma.2019.112790

[41] Baton J, Geslin W, Moussa C (2021) Influence of pre-recovery on the recrystallization of pure tantalum. J Mater Sci 56:15354–15378. https://doi.org/10.1007/s10853-021-06218-0

[42] Kedharnath A, Kapoor R, Sarkar A (2023) Evolution of dislocations and grain boundaries during multi-axial forging of tantalum. Int J Refract Metal Hard Mater 112:106120. https://doi.org/10.1016/j.ijrmhm.2023.106120

[43] Weinberger CR, Boyce BL, Battaile CC (2013) Slip planes in bcc transition metals. Int Mater Rev 58:296–314. https://doi.org/10.1179/1743280412Y.0000000015

[44] Pande CS, Masumura RA, Armstrong RW (1993) Pile-up based hall-petch relation for nanoscale materials. Nanostruct Mater 2:323–331. https://doi.org/10.1016/0965-9773(93)90159-9

[45] John JL, Hirth P (1992) Theory of dislocations, 2nd edn. Krieger Publishing Company, Malabar. https://doi.org/10.1016/0502-8205(49)90004-0

[46] Fressengeas C, Beausir B, Kerisit C, Helbert AL, Baudin T, Brisset F, Mathon MH, Besnard R, Bozzolo N (2018) On the evaluation of dislocation densities in pure tantalum from EBSD orientation data. Mater Techn 10:6. https://doi.org/10.1051/mattech/2018058